

**AN OPTIMAL REGION OF INTEREST LOCALIZATION
USING EDGE REFINEMENT FILTER AND ENTROPY-BASED
MEASUREMENT FOR POINT SPREAD FUNCTION ESTIMATION**

AHMAD HUSNI BIN MOHD SHAPRI

UNIVERSITI SAINS MALAYSIA

2019

**AN OPTIMAL REGION OF INTEREST LOCALIZATION
USING EDGE REFINEMENT FILTER AND ENTROPY-BASED
MEASUREMENT FOR POINT SPREAD FUNCTION ESTIMATION**

by

AHMAD HUSNI BIN MOHD SHAPRI

**Thesis submitted in fulfillment of the
requirements for the degree of
Doctor of Philosophy**

October 2019

ACKNOWLEDGEMENT



Alhamdulillah, all praises to Allah for the strengths and His blessing in completing this thesis after seven years of journey. I would like to express my appreciation and thanks to my supervisor Prof. Dr. Mohd Zaid Abdullah.

Special recognition to my father Hj. Mohd Shapri bin Hussin and my mother Hjh. Inson binti Kantan for encouraging me and always being there for me. I would like to thank my in-laws, Abdul Rahman bin Abu Bakar and Wan Pазiah binti Wan Mohd Amin, for giving me endless love and inspiration. Words cannot express how beholden I am for all of the sacrifices that you all have made on my behalf. Your prayer for me was what sustained me so far.

Finally, a very special thanks to my family, especially my dearest wife Norazeani binti Abdul Rahman, and my princes and princesses; Ahmad Raif, Nur Zahra, Ahmad Zarif, and Nur Wafa for their understanding, endless support and infinite patience.

TABLE OF CONTENTS

	Page
ACKNOWLEDGEMENT	ii
TABLE OF CONTENTS	iii
LIST OF TABLES	vi
LIST OF FIGURES	vii
LIST OF ABBREVIATIONS	xiv
LIST OF SYMBOLS	xvii
ABSTRAK	xviii
ABSTRACT	xx
CHAPTER ONE: INTRODUCTION	
1.1 Introduction	1
1.2 Problem Statement	8
1.3 Objectives	12
1.4 Research Scope	12
1.5 Thesis Organization	13
CHAPTER TWO: LITERATURE REVIEW	
2.1 Introduction	15
2.2 Edge Detection in Digital Images	16
2.3 Image Contrast Enhancement	21
2.4 Concept of Region of Interest	27
2.5 Entropy and Information Theory	30
2.6 Point Spread Function Estimation	33
2.7 Blind Image Deconvolution	37

2.8	Review of Edges in Blind Image Deconvolution	39
2.9	Summary	64

CHAPTER THREE: METHODOLOGY

3.1	Introduction	65
3.2	Greyscale Transformation	67
3.3	CLAHE Enhancement	67
3.4	Edge Refinement Filter	68
3.5	Edge Detection	73
3.6	Morphological Processing	74
3.7	Partitioning and Localization	76
3.8	Entropy Calculation	78
3.9	Implementation Details	79
3.10	Test Images	82
3.11	Image Quality Indices	85
3.12	Summary	87

CHAPTER FOUR: RESULTS AND DISCUSSION

4.1	Introduction	89
4.2	Preliminary Result	89
4.3	ROI Size Evaluation	91
4.4	CLAHE Enhancement Evaluation	92
4.5	Gaussian Parameters	95
4.6	Edge Evaluation from Dataset I	97
4.7	ROI Evaluation from Dataset II	105
4.8	ROI Evaluation from Dataset III	112
4.9	Summary	117

CHAPTER FIVE: CONCLUSION AND FUTURE WORK

5.1	Conclusion	118
5.2	Recommendation for Future Work	120

REFERENCES	121
-------------------	-----

APPENDICES

APPENDIX A: Full Results from Dataset I

APPENDIX B: Full Results from Dataset II

LIST OF PUBLICATIONS AND AWARD

LIST OF TABLES

		Page
Table 4.1	Edge evaluation results comparing the proposed and established methods.	102
Table 4.2	ROI evaluation results comparing the proposed and established methods.	105

LIST OF FIGURES

		Page
Figure 1.1	The process of restoring degraded images.	6
Figure 1.2	Example of single-parameter parametric blur models and their spectra, (a-b) Gaussian blur, (c-d) diffraction by circular aperture, (e-f) uniform out-of-focus blur and (g-h) uniform linear motion blur.	7
Figure 1.3	Deblurring results with different regions of the image, (a) blurred image and ground truth PSF kernel, (b) deblurring result using whole image, (c) deblurring result using a selected square region, (d) deblurring result using another selected square region. Small square block located on bottom right-hand corner of each deblurring result corresponds to estimated PSF kernel.	9
Figure 2.1	Spatial derivative of 7×7 pixels with excluded border pixels for derivative calculation. (a) Intensity values for pixels of an image, (b) partial derivative to x direction, (c) partial derivative to y direction and (d) spatial derivative of pixels.	17
Figure 2.2	Spatial derivative of an image. (a) Original image, (b) partial derivative to x direction, (c) partial derivative to y direction and (d) spatial derivative of image.	18
Figure 2.3	Clip point and redistribution.	25
Figure 2.4	Bilinear interpolation within blocks.	26
Figure 2.5	Area of ROI in an image.	27

Figure 2.6	Two point objects being imaged by pin-hole camera.	33
Figure 2.7	Two point objects imaged by a finite aperture thin lens camera.	34
Figure 2.8	Example of Airy pattern.	35
Figure 2.9	The convolution of the PSF with a point object.	36
Figure 2.10	Flowchart of the single channel BID method by Zhou et al. (2015).	39
Figure 2.11	(a) Blur images, the deblurring results of (b) Shan et al. (2008), (c) Fergus et al. (2006) and (d) Jia (2007). The yellow rectangles indicate the selected patches for estimating kernels in (c) and the windows for computing alpha mattes and estimating kernels in (d) respectively. The estimated kernels are shown in the small bottom-right rectangles.	41
Figure 2.12	Example of edge prediction using Joshi et al. (2008), (a) a blurry city building image with edge prediction and (b) the predicted values.	44
Figure 2.13	Patch selection method using game theory (Lin et al., 2015).	49
Figure 2.14	Experimental results, (a) Original standard image Peppers, (b) Blurred image, Image recovered; (c) by TV, (d) by Li et al. (2016) (e) by Krishnan et al. (2011), and (f) by Wen et al. (2016).	51
Figure 2.15	(a) Clear image and its neighboring patches and (b) Blurred image and its corresponding patches.	53

Figure 2.16	Flowchart of the Hu and Yang (2015) algorithm.	54
Figure 2.17	Experimental result for deblurring using ROI location (square box) selected by (a) user handpicked, (b) Fergus et al. (2006), (c) Hu and Yang (2015) and (d) Li et al. (2016) method. Small square block located on the top left-hand corner corresponds to PSF estimated using a given ROI.	56
Figure 2.18	The comparison results, (a) Blurred input image, (b) Xu and Jia (2010), (c) Pan et al. (2013) and (d) Zhang and Tian (2017) algorithm. The small square box at the lower right corner of the image (b-d) is the estimated kernel.	57
Figure 2.19	Flowchart of a region selection based on RTV by Li et al. (2018).	62
Figure 2.20	Flowchart of the salient patch-based algorithm by Ma et al. (2018).	63
Figure 3.1	Flowchart of the proposed method.	66
Figure 3.2	The CLAHE example, (a) original greyscale image and (b) image after contrast enhancement using CLAHE.	68
Figure 3.3	Gaussian curve with a two-dimensional domain.	72
Figure 3.4	Example image after edge detection using Canny.	73
Figure 3.5	Example image after dilation operation.	76
Figure 3.6	Flowchart of the proposed partitioning and localization.	77

Figure 3.7	The example of (a) ROI partitioning process and (b) three possible ROI locations after partitioning and localization.	78
Figure 3.8	Test images in Dataset I, the ground-truth (a-b) images and contours from Arbelaez et al. (2011), and (c) 8 kernels from Levin et al. (2011).	82
Figure 3.9	Test images in Dataset II, the ground-truth (a) images from Hu and Yang (2015) and (b) 4 kernels from Levin et al. (2011).	84
Figure 3.10	Test images in Dataset III, (a) atypical blurred image, and (b-c) images taken from Whyte et al. (2014).	85
Figure 4.1	The preliminary BID results, (a-b) ROI located at the plain surface and its restored image, (c-d) random ROI location and its restored image. Small square block located on the top left-hand corner of (b) and (d) corresponds to PSF estimated using a given ROI.	90
Figure 4.2	Evaluation of ROI size in terms of the entropy measure, comparing proposed and established methods.	92
Figure 4.3	Results comparing entropies calculated with and without CLAHE.	93
Figure 4.4	Example of image restoration of IMG9 comparing (a) with CLAHE, and (b) without CLAHE. In this case (i) and (ii) are original and restored images respectively. Square boxes in (i) show the ROI locations and the circle areas in b(ii) highlight the ringing artefacts.	94

Figure 4.5	Edge detection results of selected blurred image using the proposed method with 3×3 filter size for various σ values, (a) $\sigma = 0.3$, (b) $\sigma = 0.5$, (c) $\sigma = 0.7$ and (d) $\sigma = 0.9$.	95
Figure 4.6	Edge detection results of selected blurred image using the proposed method with $\sigma = 0.3$ for various filter sizes, (a) 3×3 , (b) 5×5 , (c) 7×7 , (d) 9×9 , (e) 19×19 and (f) 29×29 .	96
Figure 4.7	Edge detection results of 3 selected blurred images from Dataset I. (a)(i-iii) ground truth images, (b)(i-iii) ground truth edges, (c)(i-iii) blurring kernels, (d)(i-iii) blurred input images, (e)(i-iii) edge detected images using Sobel, (f)(i-iii) edge detected images using LoG, (g)(i-iii) edge detected images using Canny's method, (h)(i-iii) edge detected images using He et al. (2013) and (i)(i-iii) edge detected images using the proposed method.	99
Figure 4.8	Selected edge detection results from Dataset I comparing (a) ground truth edges, (b) He at al. (2013) method and (c) the proposed method. Three circles locate the major differences in detected edges compared to ground truth edges.	101
Figure 4.9	PFoM edge detection results from Dataset I.	103
Figure 4.10	TCGT edge detection results from Dataset I.	104
Figure 4.11	PSNR ROI evaluation results from Dataset II.	106
Figure 4.12	KS index ROI evaluation results from Dataset II.	107

Figure 4.13	Selected test images from Dataset II that contain many repeated but identical patterns, (a) IMG2, (b) IMG6 and (c) IMG10.	108
Figure 4.14	ER ROI evaluation results from Dataset II.	109
Figure 4.15	Image restoration results of selected blurred images from Dataset II. (a-b)(i-ii) pair of ground truth and its blurred version together with kernel responsible for blurring, (c-d)(i-ii) restored image using default ROI location, (e-f)(i-ii) restored image ROIs estimated by Hu and Yang (2015), (g-h)(i-ii) restored image ROIs estimated by Ma et al. (2018), (i-j)(i-ii) restored image ROIs estimated by Li et al. (2018) and (k-l)(i-ii) restored image ROIs estimated by the proposed method.	111
Figure 4.16	Image restoration results using Dataset III. (a)(i-ii) default ROI location and its deblurring result, (b)(i-ii) ROI estimated using Hu and Yang (2015) and its deblurring result, (c)(i-ii) ROI estimated using Ma et al. (2018) and its deblurring result, (d)(i-ii) ROI estimated using Li et al. (2018) and its deblurring result, and (e)(i-ii) ROI estimated using the proposed method and its deblurring result. Small square block located on top left-hand corner of each restored result corresponds to estimated kernel using a given ROI.	113
Figure 4.17	Image restoration results using Dataset III. (a)(i-ii) default ROI location and its deblurring result, (b)(i-ii) ROI estimated using Hu and Yang (2015) and its deblurring result, (c)(i-ii) ROI estimated using Ma et al. (2018) and its deblurring result, (d)(i-ii) ROI estimated using Li et al. (2018) and its deblurring result, and (e)(i-ii) ROI estimated using the proposed method and its deblurring result. Small square block located on top left-hand corner of each restored result corresponds to estimated kernel using a given ROI.	115

Figure 4.18 Image restoration results using Dataset III. (a)(i-ii) default ROI 116 location and its deblurring result, (b)(i-ii) ROI estimated using Hu and Yang (2015) and its deblurring result, (c)(i-ii) ROI estimated using Ma et al. (2018) and its deblurring result, (d)(i-ii) ROI estimated using Li et al. (2018) and its deblurring result, and (e)(i-ii) ROI estimated using the proposed method and its deblurring result. Small square block located on top left-hand corner of each restored result corresponds to estimated kernel using a given ROI.

LIST OF ABBREVIATIONS

AHE	Adaptive Histogram Equalization
ALM	Augmented Lagrangian Method
BID	Blind Image Deconvolution
BCCB	Block Circulant with Circulant Blocks
BTTB	Block Toeplitz with Toeplitz Block
BC	Boundary Condition
BBHE	Brightness Preserving Bi-Histogram Equalization
CG	Conjugate Gradients
CGLS	Conjugate Gradients Least Squares
CLS	Constrained Least Squares
CBIR	Content Based Image Retrieval
CVC	Contextual and Variational Contrast Enhancement
CLAHE	Contrast Limited Adaptive Histogram Equalization
CNN	Convolutional Neural Network
CDF	Cumulative Distribution Function
DFT	Discrete Fourier Transform
DoG	Difference of Gaussians
DSIHE	Equal Area Dualistic Sub-Image Histogram Equalization
ER	Error Ratio
ESIHE	Exposure Based Sub-Image Histogram Equalization
FFT	Fast Fourier Transform
GMM	Gaussian Mixture Model
GCV	Generalized Cross-Validation

HE	Histogram Equalization
HVS	Human Visual System
KS	Kernel Similarity
LS	Least Squares
MAP	Maximum a-Posteriori Estimation
MSE	Mean Square Error
MFSR	Multi-Frame Super-Resolution
MMBEBHE	Minimum Mean Brightness Error Bi-Histogram Equalization
NGM	Nondimensional Gaussianity Measure
PFoM	Pratt's Figure of Merit
PSO	Particle Swarm Optimization
PMMW	Passive Millimeter-Wave
PSNR	Peak Signal-to-Noise Ratio
PSF	Point Spread Function
PDF	Probability Density Function
RANSAC	Random Sample Consensus
RBIR	Region Based Image Retrieval
RGB	Red-Green-Blue
ROI	Region of Interest
RTF	Regression Tree Fields
RTV	Relative Total Variation
SSDHE	Segment-Selective Dynamic Histogram Equalization
SVD	Singular Value Decomposition
SDR	System Designated ROI
TBIR	Text Based Image Retrieval

TCGT	Twofold Consensus Ground Truth
TV	Total Variational
UDR	User Designated ROI
VD	Variational Dirichlet

LIST OF SYMBOLS

cp	Clip Point
T	Remapping Function
cdf	Cumulative Distribution Function
pdf	Probability Density Function
$H(\cdot)$	Heaviside Step Function

**PENYETEMPATAN KAWASAN BERKEPENTINGAN OPTIMUM
MENGUNAKAN PENAPIS PENAMBAHBAIKAN PINGGIR DAN
PENGUKURAN BERASASKAN ENTROPI UNTUK PENGANGGARAN
FUNGSI PENYEBARAN TITIK**

ABSTRAK

Penggunaan pinggir bagi menentukan lokasi kawasan berkepentingan (ROI) optimum menjadi semakin popular dalam penyahkabur imej. Kajian terkini menunjukkan bahawa kawasan dengan pinggir yang jelas cenderung menghasilkan keputusan penyahkabur yang lebih baik. Dalam kajian ini, kaedah langsung bagi penyetempatan ROI berdasarkan penapis penambahbaikan pinggir dan pengukuran berasaskan entropi telah dicadangkan. Dengan menggunakan kaedah ini, kebarangkalian taburan skala kelabu dapat diukur secara kuantitatif berdasarkan lokasi ROI yang ditentukan. Kaedah ini hanya melibatkan kos pengiraan yang rendah kerana ia tidak mengandungi operasi pengiraan matriks. Kaedah yang dicadangkan telah diuji menggunakan tiga set imej ujian - Dataset I, II dan III. Keputusan empirikal mencadangkan bahawa penapis penambahbaikan pinggir yang diperkenalkan adalah kompetitif apabila dibandingkan dengan kaedah-kaedah pengesanan pinggir yang sedia ada dan mencapai prestasi yang lebih baik dalam angka merit Pratt (PFoM) dan nilai kebenaran latar konsensus berganda (TCGT); purata pada 15.7 % dan 28.7 %. Keberkesanan kaedah yang dicadangkan ini terletak pada penggunaan strategi penapisan yang lebih baik dalam menganggarkan fungsi penyebaran titik (PSF), dan seterusnya, pemulihan imej yang lebih tepat. Hasilnya, penyelesaian yang dicadangkan dibandingkan dengan baik terhadap teknik-teknik sedia ada dengan purata nisbah isyarat ke bunyi (PSNR), indeks kekerapan kernel (KS), dan nisbah ralat (ER) pada 24.8 dB, 0.6 dan 1.4. Eksperimen-eksperimen tambahan yang melibatkan

imej kabur sebenar menunjukkan daya saing kaedah yang dicadangkan dalam melakukan pemulihan tanpa PSF.

**AN OPTIMAL REGION OF INTEREST LOCALIZATION
USING EDGE REFINEMENT FILTER AND ENTROPY-BASED
MEASUREMENT FOR POINT SPREAD FUNCTION ESTIMATION**

ABSTRACT

The use of edges to determine an optimal region of interest (ROI) location is increasingly becoming popular for image deblurring. Recent studies have shown that regions with strong edges tend to produce better deblurring results. In this study, a direct method for ROI localization based on edge refinement filter and entropy-based measurement is proposed. Using this method, the randomness of grey level distribution is quantitatively measured, from which the ROI is determined. This method has low computation cost since it contains no matrix operations. The proposed method has been tested using three sets of test images - Dataset I, II and III. Empirical results suggest that the improved edge refinement filter is competitive when compared to the established edge detection schemes and achieves better performance in the Pratt's figure-of-merit (PFoM) and the twofold consensus ground truth (TCGT); averaging at 15.7 % and 28.7 %, respectively. The novelty of the proposed approach lies in the use of this improved filtering strategy for accurate estimation of point spread function (PSF), and hence, a more precise image restoration. As a result, the proposed solutions compare favourably against existing techniques with the peak signal-to-noise ratio (PSNR), kernel similarity (KS) index, and error ratio (ER) averaging at 24.8 dB, 0.6 and 1.4, respectively. Additional experiments involving real blurred images demonstrated the competitiveness of the proposed approach in performing restoration in the absent of PSF.

CHAPTER ONE

INTRODUCTION

1.1 Introduction

Images in everyday life are everywhere. The world's observations in the form of graphics are desirable and represent the capabilities of a human visual system. Photographic images obtained are valuable and in this case, images can be interpreted as scenes to be observed or visually observable objects. However, imaging is imperfect with the existence of blur, noise, ambiguity in measurement and many other degradations, just like other observation processes. Intrinsically, imaging is a procedure of discarding information where the real world is projected to the lower-dimensional imaging medium. Occasionally the missing information may be useful to summarize the essential scene that produces this observation.

According to Chan and Shen (2005), image acquisition, processing, and interpretation are three independent modules in imaging sciences. Summary of these modules will be briefly discussed even though the main effort of this thesis depends on image processing. All physical mechanisms including algorithms and mathematical models involved in the process of image generation are called image acquisition, such as human vision. Image formation system for human vision contains the lens, iris, pupil, cornea, cone, and rods. On average, light can be captured in wavelength between 400-700 nm using the human vision system.

Meanwhile, the extraction of useful information from the image using a variety of procedures is called image processing. It is categorized as signal processing where the image as an input and output may be image or features related to that image. Hence, image processing has become the core of the research area in computer science and engineering. Finally, image interpretation is a definitive objective in imaging sciences. The ability to interpret an image, by having the capacity to monitor a scene, distinguish an objective in a video and estimate its position and speed, recognizing individuals, are examples of image interpretation tasks, also known as computer vision.

Image restoration research started with the early space programs in the 1960s as stated by Banham and Katsaggelos (1997). Considering the cost and impact related with obtaining the images from the spacecraft, the degradation of the information was not a negligible issue. Consequently, there was a critical requirement for processing methods that could correct and revert the unwanted impacts due to suboptimal systems, mechanical vibrations, movement, and many others. Albeit these days this approach towards image processing is as yet restricted for the top of the line applications, such as, space science and medical imaging, its utilization in consumer electronics is increasingly gaining attention. More processing power is accessible in these devices and users are more mindful of image quality on non-dedicated imaging platforms, like camera phones.

The field of image restoration has seen enormous growth in interest over the last two decades. There are numerous astounding overview articles, journal papers, and course readings regarding the matter of image restoration and identification (Bovik, 2009; Gonzalez and Woods, 2007; Hansen et al., 2006). Various different algorithms have been proposed and seriously considered for accomplishing a fast

recovered and high resolution reconstructed images (Lagendijk and Biemond, 2009). The recovery of an original image from degraded observations is of urgent significance and discovers application in several scientific areas including medical imaging, astronomical imaging, remote sensing, and military surveillance.

One of the fields of image restoration is called image deblurring or image deconvolution. Image deblurring is concerned about the reconstruction or estimation of the uncorrupted image from a blurred one (Bovik, 2009). In other words, image deblurring is the process of removing blurring artefacts from images, such as blur caused by defocusing aberration or motion blur. On a very basic level, it tries to execute an operation on the image that is the inverse of the imperfections or blurs in the image formation system. In the utilization of image restoration strategies, the characteristics of the degrading system are thought to be known a priori. However, in much practical application, this condition is difficult to be fulfilled. Therefore, some kind of estimation is needed in order to perform a restoration. The blur is typically modelled as the convolution of a point spread function (PSF) with a hypothetical sharp input image (which is to be recovered), where both the sharp input image and the PSF are unknown. This is an example of an inverse problem. In almost all cases, there is insufficient information in the blurred image to uniquely determine a plausible original image, making it an ill-posed problem.

The goal of blur identification is to assess the properties of the real imaging system from the observed degraded image itself before the restoration procedure. The blend of blur identification and image restoration is frequently alluded to as blind image deconvolution (BID) (Kundur and Hatzinakos, 1996). On the other hand, the non-image deconvolution needs earlier learning of the degradation process.

Degradation can be evaluated in light of image observation, by modelling and experiments (Gonzalez and Woods, 2007).

The PSF may be determined in a variety of ways. For example, if one is imaging a star field through a telescope and recorded on a camera via long exposure, then the motion of the star images may be determined knowing the rotation rate of the Earth, as well as the location, orientation, and field of view of the telescope (Nagy and O'Leary, 1998). Another example of recent work in estimating the PSF is with blurry images resulting from camera shake. Normally, the precise motion of the photographer's hand during exposure would not necessarily be known. However, modern schemes use a portion of the image with distinct features such as a sign with letters, can be used to estimate a PSF (Hirsch et al., 2011; Joshi et al., 2008). Similarly, researchers have used the accelerometer and gyroscope information captured during a camera exposure on modern smartphones to generate a PSF (Joshi et al., 2010). If the PSF is not known a priori, then an added layer of complexity in the deblurring process is introduced, as the PSF must be estimated. If there is no external information on which to base the estimate of the PSF, then the process reverts to BID where the PSF must be estimated and applied in a recursive manner (Harmeling et al., 2010).

After estimating the PSF, some recovery procedures can be utilized for deconvolution, including the algebraic and transform related restoration techniques. Transform related restoration techniques include breaking down the degraded image after a suitable transform has been used. By acting specifically on the transformed image before applying an inverse transform, or utilizing the transformed image data to build up an inverse filter, an image might be halfway recovered.

Al-Rubaye (2018) reviewed some of the techniques related to the transformation, including inverse filters, Wiener filters, parametric estimations, Kalman filters, and homomorphic filters. On the other hand, efforts involve finding direct solutions to malfunctioning matrix inversion techniques, or techniques involving recurring methods to reduce degradation measurement are called algebraic techniques. It can be classified into techniques such as pseudoinverse, Wiener estimation and singular value decomposition (SVD) pseudoinverse spatial and constrained image restoration.

BID based on the total variational (TV) minimization technique is powerful to recover edges of images and also some blurring functions, for example, out-of-focus blur and motion blur (Chan and Wong, 2004). You and Kaveh (1999) introduced anisotropic regularization systems to exploit the piecewise smoothness of the image and the PSF. The end goal is to moderate the serious absence of data experienced in blind restoration of shift-invariant and shift-variant blurred images. These methods are shown on linear motion blur and out-of-focus blur. Edge protecting regularization techniques, with regards to image restoration and denoising, are discussed in Rakha (2004).

Images are expected to document valuable data, yet the nearness of the blur is unavoidable. Motion blur is the impact caused by relative movement between the camera and the scene amid image exposure time. Restoration of motion-blurred images has been a crucial issue in advanced imaging for quite a while (Cai et al., 2009). Usually, the process of restoring degraded images can be broken down into three major steps as shown in Figure 1.1. In the first step, information about the blurring and noise is used to create a model of the degraded image. By at large of image restoration

strategies utilize the linear image degradation model. In the second step, information about the original and degraded images are used to formulate an objective function that, when solved, removes the blurring and noise from the degraded image. This is generally accomplished using some form of inverse function or optimization problem. In the third step, an algorithm for solving the image restoration problem is developed.

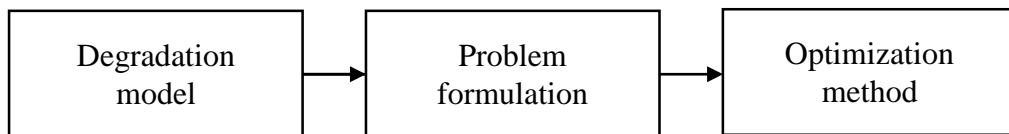


Figure 1.1: The process of restoring degraded images.

Blurring is a type of bandwidth reduction of a perfect image attributable to the imperfect image formation process. It can be caused by a relative movement between the camera and the original scene, or by an optical framework that is out-of-focus. At the point when elevated photos are created for remote sensing purposes, blurs are adapted by atmospheric turbulence, aberrations in the optical framework, and relative movement between the camera and the background. For instance, electron micrographs are corrupted by spherical aberrations of the electron lenses and computed tomography scans experience the ill effects of x-ray scatter. A few cases of single-parameter parametric blur models, formed with their Fourier spectrum, are shown in Figure 1.2.

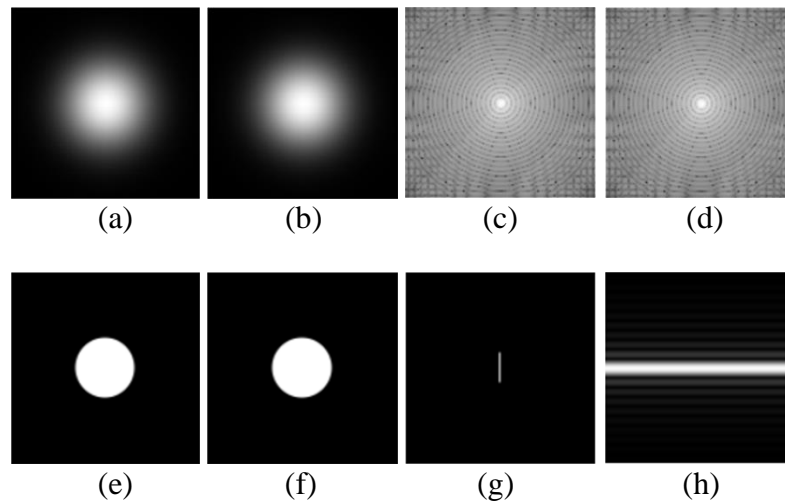


Figure 1.2: Example of parametric blur models and their spectra, (a-b) Gaussian blur, (c-d) diffraction by circular aperture, (e-f) uniform out-of-focus blur and (g-h) uniform linear motion blur.

Apart from blurring, another major concern in image deblurring is the presence of noise. Noise is any random fluctuation in pixel intensity that obscures the original image content and does not contain meaningful information. In imaging, it is usually additive or multiplicative. Noise is generally a distortion due to the imaging framework rather than to the scene recorded. The noise brings about irregular varieties to pixel values in the image. This could be caused by the imaging framework itself, or the recording or transmission medium. Noise is characterized by its frequency distribution, which will largely depend on the noise source. Common types of noise include Gaussian noise and salt and pepper noise.

1.2 Problem Statement

The blurring operation, which is linear and spatially invariant, can be expressed as a convolution. Commonly, the blurred image development process is modelled as a latent image convolved with a spatial-invariant PSF. Thus, the deblurring process is known as a two-dimensional deconvolution problem. At the point when the PSF kernel is known or has been precisely estimated, the issue is reduced to non-blind deconvolution. In contrast, if the blur kernel is unknown, the deblurring process becomes the blind deconvolution problem. The ill-posed nature of the single image deblurring setting makes the problem rather difficult.

To deblur an image, it has been demonstrated that evaluating the blur kernel or PSF first and after that taking care of a non-blind deconvolution issue with the estimated kernel renders good outcomes (Levin et al., 2009). For the single image deblurring issue, by default, it is very convenient to make full utilization of the input blurred image in PSF estimation. However, not all pixels of the input blurred image are distinctive. Smooth districts, for instance, do not contribute much in the estimation of the PSF. Hence, by extracting an optimal region of interest (ROI) for PSF estimation, a precisely estimated PSF would then be able to be utilized to recuperate a dormant clear image with high visual quality.

Preferably, the ROI should contain sufficient information needed to represent the whole blurred image. Many algorithms such as the (Šroubek and Milanfar, 2012; Krishnan et al., 2011; Khalifa et al., 2012; Rodrigues et al., 2006) assume the ROI is located at the centre of an image. This assumption holds for some types of image, especially when the details are concentrated at regions surrounding the central

location. However, it performs poorly when the details are located further away from the central location.

Latest studies have shown that regions with strong edges tend to yield better deblurring results (Maik et al., 2018; Zhao et al., 2017; Vasu and Rajagopalan, 2017). Some of the gradient-based methods favour salient edges with gradients of specific patterns (Xu et al., 2018; Yousaf and Qin, 2013; Bae et al., 2012; Cho et al., 2010; Joshi et al., 2008). Furthermore, recent work on one-dimensional signal recovery is demonstrated that edges of short length could adversely affect the deblurring results (Xu and Jia 2010). In other words, if the whole image is used for image deblurring without a deliberate selection of good features, negative impacts are likely to lead to inferior results. For this reason, along with improving computational efficiency, it is preferable to select a region, rather than the whole image, for estimating blur kernels.

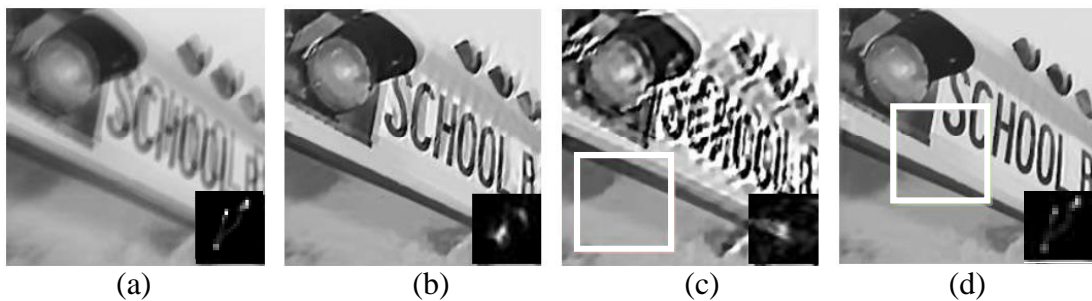


Figure 1.3: Deblurring results with different regions of the image, (a) blurred image and ground truth PSF kernel, (b) deblurring result using whole image, (c) deblurring result using a selected square region, (d) deblurring result using another selected square region. Small square block located on bottom right-hand corner of each deblurring result corresponds to estimated PSF kernel.

Figure 1.3 illustrates that different regions may lead to completely different kernel estimation results, and thereby different recovered images. This problem can often be partly alleviated by manual selection and visual inspection of the results. But, this requires tedious human inputs for deblurring images. Thus, alongside enhancing computational proficiency as well as reject soaked and uniform image locales that normally delude the estimation procedure, it is desirable over select a region, as opposed to the entire image, for estimating blur kernels (Xu and Jia, 2010; Fergus et al., 2006). Nevertheless, the methods and procedures for the questions regarding which regions or what image structures retrieving optimal ROI needed for estimating the blur kernel remain a challenge.

In addressing this problem, Hu and Yang (2015) recommend a good selection of features and patches based on machine learning to estimate the blur kernel. Good image features can be detected, which allows the blur kernel to be accurately estimated. For that purpose, the exploitation of contextual constraints between the regions of the image is formulated based on learning problems within the conditional field framework.

Recently, deep learning methods have also been successfully applied to image deblurring problems such as Chakrabarti (2016), Hradiš et al. (2015) and Xu et al. (2014). But, there are three main differences between deep learning methods and direct methods. First, all deep methods need to train deep models on a large amount of training images pairs, and it is not convenient to obtain the training dataset. Second, some of deep learning methods may have a constriction on the size of the input image, and third, the training dataset and the deep learning network should be chosen very

carefully, or else the deblurring results of deep learning will be even worse than a direct method (Ma et al., 2018).

On the contrary, a direct method only takes a single image as the input, and hence, does not require a large training dataset. Lastly, a direct method utilises image regions which are helpful for deblurring only. Therefore, this method can be regarded as a pre-process in the whole image deblurring process. According to Ma et al. (2018), it is also feasible to integrate the direct method with deep learning technique. Clearly, from this literature review, there is still room for improvement in finding a better region for PSF kernel estimation.

In addition, the use of edges in determining an optimal ROI location has become an important factor in deblurring images (Schuler et al., 2016; Wen et al., 2016; Pan et al., 2013). The promising results have been shown (Dong et al., 2017; Pan et al., 2017; Joshi et al., 2008) and it is proof that if the significant edges can be detected, more accurate PSF kernel is able to be estimated. Hence, a clear restored image can be realized using BID. Therefore, a new method in determining optimal ROI for PSF estimation is needed. In this study, the combination of edge refinement filter, image contrast enhancement, and entropy-based measurement are investigated to overcome these shortcomings and drawbacks. The idea is to use the ROI location candidates selected using edge refinement filter mapping with an enhanced image using contrast limited adaptive histogram equalization (CLAHE). The optimal ROI is determined by calculating the maximum entropy value for each ROI candidates that represented the randomness of grey-level distribution in the image. This information allows optimal or near optimal ROI to be retrieved adaptively.

1.3 Objectives

The primary objective of this research is to design and develop a solution to obtain the optimal ROI localization for PSF kernel estimation in image deblurring. In achieving this objective, the following secondary objectives are therefore set:

1. To design a spatial filter for refining important edges in the blurred images.
2. To propose entropy-based measurement as a mean for ROI localization, and hence, PSF estimation.

1.4 Research Scope

In this study, the ROI localization is applied using the proposed method by manipulating the pixels in the image plane directly. There is no training data needed since the proposed method is a direct computation method. Here, the ROI is a square block and the input is assumed to be a greyscale image. The procedures involved firstly estimating the PSF, after which the image restoration is attempted using single-channel BID. Existing algorithms are used in the computation of PSF and BID. Therefore, the accuracy of the image restoration is limited by the accuracy of these algorithms. Similarly, the blurring process is assumed to be linearly space invariant while the blurred images are produced by the convolution with kernels published by other researchers. Hence, the types of blurriness are limited to the types that these kernels produce. Furthermore, it is assumed that the no additive noise caused by a random and unwanted fluctuation of signal is presence in input image.

1.5 Thesis Organization

This thesis is organized into five chapters. Organization of the thesis chapters was set in a way that the whole project could be expressed clearly from the introduction, literature and theoretical review to the methodology of edge detection and ROI localization. The methodology leads to the main parts of the project, and finally the results and discussion, along with the conclusion and description of future work.

Chapter 2 includes the theoretical background of edge detection in digital images, with an image restoration overview including the state-of-the-art trends in BID, PSF estimation and the emergent image restoration techniques. This chapter also describes the image contrast enhancement using CLAHE. This is followed by a concept of an ROI, the entropy and information theory. Finally, some major applications of ROI extraction are discussed.

Chapter 3 focuses on the methodology of the developed and proposed technique. Steps and procedures for the optimal ROI localization at each stage are clearly explained. In addition, five figure-of-merits illustrate the performance of the outlined ROI, along with the mathematical formulation involved. Test images are also described at the end of this chapter.

Chapter 4 discusses the outcomes acquired utilizing the proposed method portrayed in the past chapter. Two main simulations will be performed to assess the performance of the proposed method. The first part explains the results of edge evaluation from Dataset I comparing the proposed edge refinement filter against standard methods and He et al. (2013) method. The second part describes the restored

image results of the proposed method compared to established methods using synthetic and real images from Dataset II and III, respectively.

Finally, Chapter 5 concludes the important contributions of this study, and highlights suggested future work.

CHAPTER TWO

LITERATURE REVIEW

2.1 Introduction

Image blur is introduced in a number of stages in a camera. The most common sources of image blur are motion, defocus, and aspects inherent to the camera, such as pixel size, sensor resolution, and the presence of antialiasing filters on the sensor. When blur is undesirable, one can deblur an image using a deconvolution method, which requires accurate knowledge of the blur kernel. In applications where blur is desirable and essential, such as shape from defocus, it is still necessary to recover the shape and size of the spatially varying blur kernel. Recovering a PSF from a single blurred image is an inherently ill-posed problem due to the loss of information during blurring. The observed blurred image provides only a partial constraint on the solution, as there are many combinations of PSFs and “sharp” images that can be convolved to match the observed blurred image.

The present chapter discusses the review of literature and background of the image restoration subjects such as the relationship between ROIs, edges and PSF estimation in the BID. It can be divided into basic theoretical understanding, methods, and concepts. Section 2.2 outlines the edge detection in digital images. Then, Section 2.3 describes an image contrast enhancement method followed by the concept of ROI in Section 2.4. The theoretical basis of entropy, PSF estimation and BID will be explained in Section 2.5, 2.6, and 2.7, respectively. Then, a review of edges in BID involving PSF estimation methods will be described in Section 2.8. Lastly, Section 2.9 summarizes this chapter.

2.2 Edge Detection in Digital Images

In a digital image, an edge is a set of connected pixels that lie on the boundary between two regions. Edge detection is one of the most commonly used tools in image processing and, hence, object-recognition. Accordingly, edge detection is the process of locating the edge pixels on the boundaries of objects that fall within a digital image (Abo-Zahhad et al., 2014). Several ways to perform edge detection have been designed to date. Edge detection operators can be classified into two major categories: gradient and Laplacian methods (Dharampal, 2015). The gradient method detects the edges by finding the maxima and minima in the first spatial derivative of the image. Mathematically, the gradient of a two-variable function (here the image intensity function) at each image point is a 2D vector with the components given by the derivatives in the horizontal and vertical directions. At each image point, the gradient vector points in the direction of largest possible intensity increase, and the length of the gradient vector corresponds to the rate of change in that direction.

Spatial derivative for a 7×7 matrix of pixel intensity values is shown in Figure 2.1. Partial derivative towards x and y -direction of the pixels (intensity values) are calculated first by applying an operator. Then gradient value $df(x, y)$ is calculated from these partial derivatives. Clearly, the derivative shows a maximum located at the centre of the edge in the original signal.

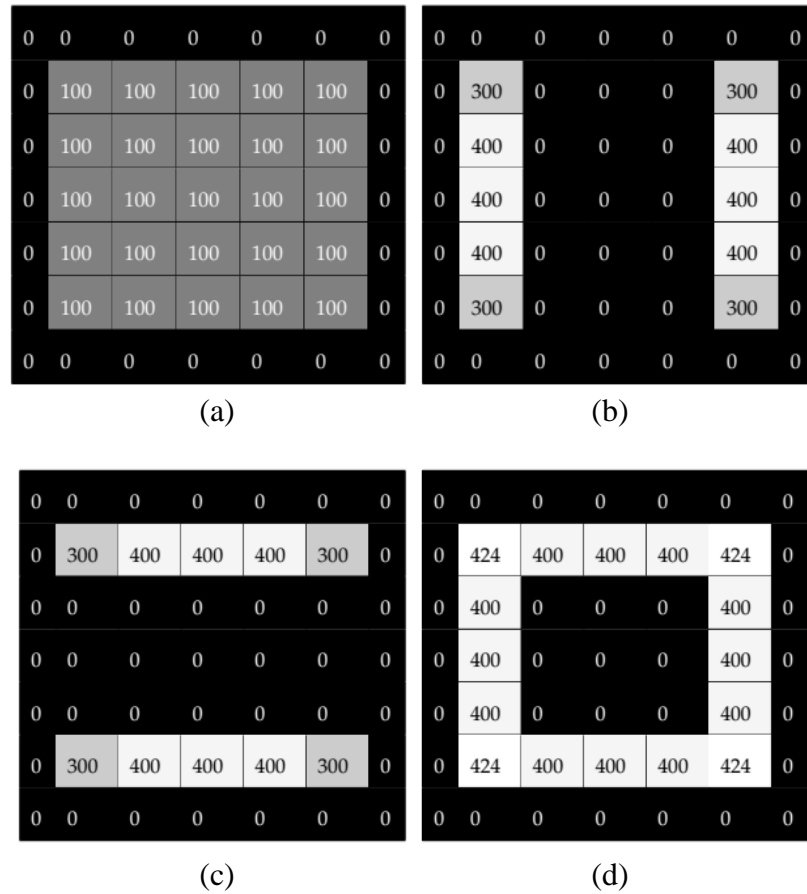


Figure 2.1: Spatial derivative of 7×7 pixels with excluded border pixels for derivative calculation. (a) Intensity values for pixels of an image, (b) partial derivative to x direction, (c) partial derivative to y direction and (d) spatial derivative of pixels.

This method of locating an edge is characteristic of the ‘gradient filter’ family of edge detection filters and includes the Sobel method. A pixel location is declared an edge location if the value of the gradient exceeds some threshold. As mentioned before, edges will have higher pixel intensity values than those surrounding it. So once a threshold is set, the gradient value can be compared to the threshold value and an edge is detected whenever the threshold is exceeded. Figure 2.2 shows images after applying different steps in a spatial derivative. Examples of this method are Roberts, Prewitt and Sobel edge detectors (Halder et al., 2019).



Figure 2.2: Spatial derivative of an image. (a) Original image, (b) partial derivative to x direction, (c) partial derivative to y direction and (d) spatial derivative of image.

Alternatively, the Laplacian method, also known as second order derivative is used to find the edges by searching for zero-crossings in the second derivative of the image. An edge has the one-dimensional shape of a ramp and calculating the derivative of the image can highlight its location. Furthermore, when the first derivative is at a maximum, the second order derivative is zero. As a result, another alternative to finding the location of an edge is to locate the zeros in the second order derivative. Second order derivative of an image can be obtained by applying a suitable operator.

Neoh and Hazanchuk (2004) defined the basis of an edge detection operator as the process of determining the level of variance between different pixels by a matrix area gradient operation. It is calculated by forming a matrix centered on a pixel chosen as the centre of the matrix area. The middle pixel in the matrix is classified as an edge when the value of this matrix area is above a given threshold.

The comparative analysis of various image edge detection methods is presented by Juneja and Sandhu (2009). The evidence for the best detector type is judged by studying the edge maps relative to each other through statistical evaluation. Upon this evaluation, an edge detection method can be employed to characterize edges to represent the image for further analysis and implementation. It has been shown that the Canny method performs better than all these operators under almost all scenarios.

The problem comes when the image is blurry, in this condition results of edge detection by using standard methods is very poor. The standard edge detection methods having difficulties in detecting edges in blurred images. For example, the Sobel method failed to highlight the edges and the Canny method suffers by the number of “false edges” when it is being used with a blurred image. Thus, a customize edge detection method for a blurred image is needed. To overcome this problem, pre-processing techniques which can solve the problem of blurriness from images are needed. Choudhary et al. (2017) proposed an edge detection method using pre-processing techniques which can find edges in blurry images. The blurriness of the image has been solved by using the Wiener filter and power spectrum function.

According to Zawaideh et al. (2017), filtering is aimed to pre-process the image in order to make it more adaptive for a specific application such as edge-preserving smoothing operator. The main purpose of filtering is to improve the visual

quality of an image or extract image attributes such as edges or contours (Kaushik and Sharma, 2012). The process of filtering can be performed by changing the level value of grey pixel within an image according to the value of its neighbours. Filtering process should obtain an image with optimal visibility by keeping the significant elements of an image (Chandel and Gupta, 2013). The neighbourhoods of the processed pixel represent the function of mask shape, which selected by the filter. Moreover, various filtering methods have been developed according to the type and the intensity of noise, while others have been developed based on the applications of which image is intended.

Ying et al. (2019) proposed the subpixel edge detection method based on cubic spline interpolation to improve the detection accuracy of the edges of the motion-blurred images. By analyzing the grayscale distribution of the object images in different motion directions, different methods have been used to enhance the low-frequency sub-band images which were obtained by wavelet transform. Experimental results show that the proposed method avoids the misdetection of the edges of the blurred image, and obtains higher edge detection accuracy.

Meanwhile, a localizing edges method for estimating PSF by removing outlier points using the Random Sample Consensus (RANSAC) algorithm has been introduced by Li et al. (2016). The method accomplished by analyzing the profile at an edge point along the normal direction to an edge, and then utilize RANSAC to rule out the outlier maximum and minimum edge points. Experimental results show that the proposed method is able to locate edges more accurately than the subpixel difference of Gaussians (DoG) and the Canny method.

Unimportant edge information makes kernel estimation sensitive to noise, and weak edges are easily influenced by a blur (Xu and Jia, 2010). Thus, a fuzzy edge prediction method has been proposed by Li et al. (2016) to extract stable edges from a blurred image and then obtain highly accurate kernel estimation results. This approach is based on the intuitive knowledge that stable edges can yield a steady prior for kernel estimation. With this prior, the proposed method can accurately obtain a latent image in a pyramid structure to reduce computational complexity.

He et al. (2013) proposed the guided filter which is an edge-preserving smoothing operator similar to the popular bilateral filter (Tomasi and Manduchi, 1998). However, it is much more efficient and has better behaviour near the image edge. Researchers have successfully used guided image filter in many applications such as image fusion (Dong et al., 2018), image dehazing (Liu et al., 2019), image smoothing (Zhu et al., 2019), edge-preserving smoothing (Yang et al., 2018) and saliency region detection (Sun et al., 2015). For further insights, the guided image filtering will be discussed in the next chapter.

2.3 Image Contrast Enhancement

Contrast enhancement is a standout amongst the most imperative methods for image enhancement (Kotkar and Gharde, 2013). In this method, the contrast of an image is enhanced to improve the image for human vision. The term contrast is the separation of dark and bright areas presented in the image. Contrast enhancement can be considered as local and global contrast enhancement. Global contrast enhancement methods are quick and straightforward and are appropriate for the general

improvement of the image. These systems cannot adjust to local splendor highlights of the input image in light of the fact that sole global histogram data over the entire image is utilized (Kong et al., 2013). This reality confines the contrast ratio in a few sections of the image and subsequently causes critical contrast misfortunes in the background and other small districts. A standout amongst the most broadly utilized algorithms is histogram equalization (HE), the essential thought of which is to alter the intensity histogram to approximate a uniform distribution (Lee and Tseng, 2017). It treats all areas of the image similarly and, in this way regularly yields poor local execution regarding a point of interest safeguarding of image.

A few other local contrast enhancement procedures are additionally utilized. Local enhancement methods can improve general contrast the more reliance. In local enhancement, a small window slides through each pixel of the input image consecutively and only those blocks of pixels are enhanced which fall under in this window. After that grey level mapping is done for pixels which lie in that window (Gupta and Kaur, 2014). In this manner, it makes great utilization of local data. In any case, in local enhancement techniques, the computational cost goes high because of its completely covered sub-pieces and causes over-upgrade in a few segments of the image. Another issue is that it upgrades the noise impact in the image as well.

The inherent shortcoming of HE is over-enhancement in images with a large smooth area, which results in unnaturalness and wash-out appearance. Dark images captured under low light condition contain the large smooth area with a narrow dynamic range, and thus HE causes over-enhancement after contrast enhancement. In the last decades, several refinement approaches have been proposed, such as brightness preserving bi-histogram equalization (BBHE) (Kim, 1997), equal area

dualistic sub-image histogram equalization (DSIHE) (Wang et al., 1999), and minimum mean brightness error bi-histogram equalization (MMBEBHE) (Chen and Ramli, 2003). To overcome the problems of conventional HE, Celik and Tjahjadi (2012) used a Gaussian mixture model (GMM) to model the intensity distribution.

GMM plays a role in obtaining different intervals corresponding to different regions of the input image. Cheng and Huang (2013) proposed a method based on histogram modification and bilateral Bezier curve. This method utilized a Bezier curve to modify the cumulative distribution function (CDF) for smoother results. However, if the slope of the CDF at dark regions was excessively small, under-enhancement in dark regions was inevitable due to the property of the Bezier curve. Instead of using the first-order statistics, some researchers exploited the spatial information in images. Contextual and variational contrast enhancement (CVC) (Celik and Tjahjadi, 2012) applied a 2-D histogram to adjust different images, and thus images with high contrast were enhanced not as much as those with low contrast. Shu and Wu (2013) employed a joint probability with spatial information to overcome the limitation of the histogram in contrast enhancement. These two methods (Celik and Tjahjadi, 2012; Shu and Wu, 2013) achieved better performance in contrast enhancement but caused under enhancement in dark regions. Thus, they are not suitable for image enhancement of non-uniform illumination. A pivotal issue is to preserve both naturalness and features in image enhancement without under(over)-enhancement.

Multiple segmentation approaches divide the histogram of the input image into several non-overlapping sub-histograms using mean or median values as a threshold. Exposure-based sub-image histogram equalization (ESIHE) (Singh and Kapoor, 2014) redistributed the histogram by setting clip points, while segment-selective dynamic

histogram equalization (SSDHE) (Khan et al., 2014) adjusted the dynamic range by an expansion strategy. In practice, they successfully performed contrast enhancement, but noise was also enhanced.

CLAHE is locally adaptive contrast enhancement technique. It is an enhanced variant of adaptive histogram equalization (AHE) method. The AHE has a practical impediment that homogenous locales of an image can cause over-amplification of noise in light of the fact that the limited scope of pixels is mapped to a whole visualization range. CLAHE was produced to incapacitates the over-amplification issue of HE by limiting noise-like antiquities inhomogeneous districts. CLAHE limits the amplification of noise in the image with the goal that the image seems more normal. This method is likewise extremely valuable for video broadcasting where brightness necessity is high. CLAHE improves splendor level to a particular range and consequently encourages the correlation of various regions of an image (Gupta and Kaur, 2014).

In CLAHE, the image is divided into similarly measured non-overlapping rectangular locales and HE is performed in every area. Precisely, CLAHE contains five main procedures. First, the image is decomposed into equally-sized rectangular blocks, and histogram adjustment is performed in each block. Histogram adjustment includes histogram creation, clipping, and redistribution. Then, the mapping function is obtained by the CDF of the clipped histogram. Finally, bilinear interpolation is performed between the blocks to remove possible block artefacts.